Observing Tsunamis in the Ionosphere Using Ground Based GPS Measurements

D A. Galvan, A. Komjathy, Y. Tony Song, P. Stephens

Jet Propulsion Laboratory, California Institute of Technology

M. P. Hickey

Embry Riddle Aeronautical University

J. Foster

University of Hawaii at Manoa

BIOGRAPHIES

David A. Galvan is a Caltech Postdoctoral Researcher at the NASA Jet Propulsion Laboratory. He has studied magnetospheric and ionospheric physics, especially the density structure and dynamics of the Earth's plasmasphere. He is interested in coupling mechanisms between the ocean, atmosphere, ionosphere and magnetosphere. He earned his Ph.D. in Geophysics and Space Physics from UCLA in 2009.

Attila Komjathy is a senior member and principal investigator at the Ionospheric and Atmospheric Remote Sensing (IARS) group of the Tracking Systems and Applications Section at NASA's Jet Propulsion Laboratory (JPL), California Institute of Technology. He specializes in various aspects of remote sensing techniques. He received his Ph.D. from the Department of Geodesy and Geomatics Engineering of the University of New Brunswick, Canada in 1997.

Michael Hickey is a Professor of Physics and an Associate Dean at Embry-Riddle Aeronautical University, which he joined in 2002. He specializes in the numerical modeling of acoustic-gravity wave propagation in the atmosphere, and has developed a spectral full-wave model to simulate wave propagation from the lower to the upper atmosphere and coupling with the ionosphere. He obtained his Ph.D. in Space Physics in 1986 from La Trobe University, Melbourne, Australia.

Dr. Y. Tony Song is a research scientist in Oceanography at NASA's Jet Propulsion Laboratory in Pasadena, Calif., where he specializes in ocean remote sensing, ocean modeling and detection of tsunamis using GPS technology. He is a science team member on two of NASA's Earth satellite missions: the Ocean Surface Topography Mission (OSTM) and the Gravity Recovery and Climate Experiment (GRACE). He has been a lead investigator on many NASA and U.S. Navy projects and has authored more than 40 peer-reviewed publications. He is also a contributing author to the 2007 Nobel Peace Prize winning IPCC report. His study on the 2004 Indian Ocean tsunami won the 2008 JPL Ed Stone Award. He is the recipient of the 2011 NASA Exceptional Scientific Achievement Medal for his pioneering work in tsunami research. He received his doctorate from Simon Fraser University, British Columbia, Canada, in 1990.

Philip Stephens is a senior member of the Ionospheric and Atmospheric Remote Sensing (IARS) group of the Tracking Systems and Applications Section at NASA's Jet Propulsion Laboratory (JPL), California Institute of Technology. He specializes in inverse problems in the ionosphere. Prior to joining JPL in 2009, Philip was an Assistant Professor of Physics at Kennesaw State University. He received his PhD in 2003 from the Department of Physics at Cambridge University, UK.

James Foster is an Assistant Researcher at the Hawaii Institute of Geophysics and Planetology in the School of Ocean and Earth Science and Technology, University of Hawaii at Manoa. His interests include Geodesy, GPS meteorology and the impact and mitigation of the atmosphere on space geodetic measurements. He earned his Ph.D. from the University of Hawaii in 2002.

ABSTRACT

Ground-based Global Positioning System (GPS) measurements of ionospheric Total Electron Content (TEC) show variations consistent with atmospheric internal gravity waves caused by ocean tsunamis following recent seismic events, including the Tohoku tsunami of March 11, 2011. We observe fluctuations correlated in time, space, and wave properties with this tsunami in TEC estimates processed using JPL's Global Ionospheric Mapping Software. These TEC estimates were band-pass filtered to remove ionospheric TEC variations with periods outside the typical range of internal gravity waves caused by tsunamis. Observable variations in TEC appear correlated with the Tohoku tsunami near the epicenter, at Hawaii, and near the west coast of North America. Disturbance magnitudes are 1-10% of the background TEC value. Observations near the epicenter are compared to estimates of expected tsunami-driven TEC variations produced by Embry Riddle Aeronautical University's Spectral Full Wave Model, an atmosphere-ionosphere coupling model, and found to be in good agreement. The potential exists to apply these detection techniques to real-time GPS TEC data, providing estimates of tsunami speed and amplitude that may be useful for future early warning systems.

INTRODUCTION

Tsunamis represent a continuing threat to human society. The tsunami of September 29, 2009 caused over 180 fatalities on the islands of Samoa, American Samoa, and Apia, and the Chilean earthquake of February 27, 2010 generated a tsunami that was observed in Hawaii, California, Japan, and New Zealand. More recently, the magnitude 9.0 earthquake of March 11, 2011 off the coast of Japan generated a tsunami that caused significant damage and loss of life in Japan and affected coasts throughout the Pacific Rim. Tsunami warning systems have gradually improved through the deployment and use of Deep Ocean Assessment and Reporting of Tsunamis (DART) buoys (http://www.ndbc.noaa.gov/dart.shtml). While essential to the task of tsunami monitoring, these in situ instruments are few, far between, and expensive (http://ioc3.unesco.org/itic/files/tsunami_detection_buoy_article.pdf). A supplementary method capable of providing real-time observation or confirmation of an offshore tsunami would be an important contribution to the tsunami early warning system. GNSS satellites and receivers can potentially provide this contribution via monitoring of ionospheric total electron content (TEC), with already-deployed instrumentation and at a relatively low cost.

Recent modeling results and observations have demonstrated that the ionospheric signature of an ocean tsunami can potentially be detected as a traveling ionospheric disturbance (TID) produced by internal gravity waves propagating obliquely upward in the atmosphere [e.g., *Occhipinti* et al., (2006, 2008), *Hickey et al.*, (2009), *Mai and Kiang* (2009), *Galvan et al.,* (2011)]. Such tsunami-driven TIDs have been observed using measurements of integrated ionospheric electron density (total electron content, or TEC) between Global Positioning System (GPS) satellites and receivers on the ground [e.g., *Artru et al.,* 2005; *Rolland et al.,* 2010; *Galvan et al.,* 2011; *Liu et al.,* 2011]. GPS receivers onboard satellites in low Earth orbit, such as the COSMIC constellation, may also be useful in observing these tsunami-driven TIDs.

There are many remaining unanswered questions regarding the reliability of detecting tsunami-driven TIDs, including how to distinguish them from TIDs of non-tsunami-driven origin, as well as factors affecting the propagation of internal gravity waves in the ionosphere. Recent models indicate that the magnitude of variations in electron density in the ionosphere due to tsunami-driven internal gravity waves can depend heavily on the local orientation of the geomagnetic field [e.g., Occhipinti et al., (2008)], as well as the direction of propagation of the tsunami itself, relative to winds in the upper atmosphere [Hickey et al., (2009)]. Such subtleties can influence our ability to detect tsunami-driven TIDs, and should be thoroughly explored via data analysis of multiple events.

We have analyzed GPS TEC observations from multiple ground-based GPS receiver networks, for several recent events including the Samoa tsunami of September 2009, the Chile tsunami of February 2010, and the Japan tsunami of March 2011. The Samoa and Chile events, along with details about our data analysis methodology, are discussed in *Galvan et al.*, [2011]. In the present paper we focus on observations of the ionospheric impact of the Tohoku tsunami of March 11, 2011, which was triggered by a Magnitude 9.0 Earthquake off the coast of Honshu, northern Japan.

We have found TEC variations consistent with tsunami-driven internal gravity waves for the Tohoku event. The perturbations, correlated in time, location, and wave properties with the tsunami, were observed in TEC measurements processed using JPL's Global Ionospheric Mapping software suite [e.g., *Komjathy et al.,* 2005]. These TEC data were band-pass filtered to remove variations with wavelengths and periods outside the typical range of internal gravity waves caused by tsunamis. Significant perturbations thought to be associated with the ocean tsunami were observed at Japan, Hawaii, and North America. These observations represent the largest magnitude ionospheric disturbance caused by a tsunami yet observed.

A brief comparison between observations and theoretical model results was also carried out for this event. The Song tsunami model for the sea-surface waveform of a tsunami [*Song*, 1997], has been used to compare the geographical position of the TID wavefronts with that of the sea-surface waves themselves. We also use the atmosphere-ionosphere coupling model of *Hickey et al.,* (2009) to estimate the expected variation in ionospheric TEC based on a sea-surface tsunami waveform measured by a DART buoy in the region of Japan. We compare this estimate to actual TEC observations from ground-based dual-frequency GPS receivers. By using a combination of tsunami model results for expected ocean wave properties and observations by tidal gauges and DART buoys, these ionosphere-atmosphere coupling models may be useful in predicting expected TEC variation during a future tsunami in a real-time scenario.

METHODOLOGY

Networks of GPS Receivers

Dual-frequency GPS receivers can detect the time delay of GPS radio signals caused by their passage through the ionosphere. This delay can be processed to produce TEC measurements. There are several major networks of ground-based, dual frequency GPS receivers that can be used for this purpose. The International GPS Service (IGS) network is a global network of over 350 continuously operating dual-frequency GPS stations. Such a global network provides widespread but sparse coverage; useful because, no matter where a tsunami occurs, there will likely be at least one GPS receiver on an island or coast in the vicinity that may be used to look for TEC variations. There are also major regional networks, such as Japan's GEONET network of over 1200 GPS stations (http://terras.gsi.go.jp/gps/geonet_top.html), the several dozen receivers in Hawaii run jointly by the University of Hawaii's Pacific GPS Facility and the USGS Volcano Obervatory, and the North American Plate Boundary Observatory (PBO) network of over 700 stations (http://pboweb.unavco.org/). These regional networks provide highly localized but very dense coverage, allowing for corroboration of observations via many GPS TEC observations in a particular region. We use these networks to study the ionospheric impact of the Tohoku earthquake and tsunami.

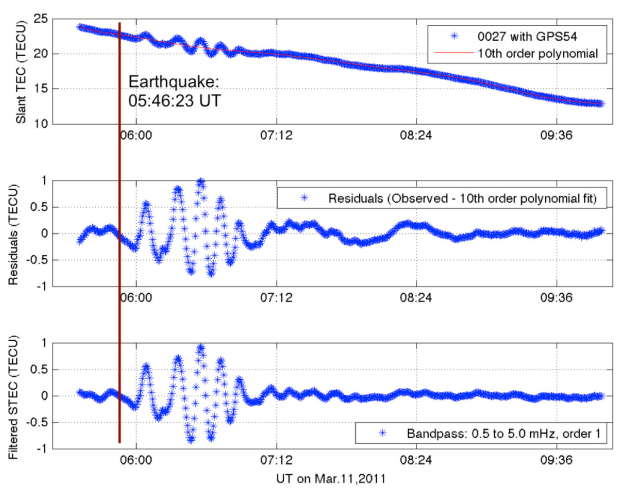

Fig 1. Time series observations of STEC (top), residuals with a polynomial fit (middle), and band-pass filtered STEC (bottom) for the arc between GEONET receiver 0027 in Japan and GPS satellite SVN 54.

GIM Processing

We use the Global Ionospheric Mapping (GIM) (*e.g., Komjathy et al.,* 2005; *Mannucci et al.,* 1998) software suite to process the Receiver Independent Exchange format (RINEX) files from networks of GPS receivers in order to produce TEC measurements between the ground receivers and GPS satellites. GIM was developed to compute high-precision ionospheric delay measurements by estimating and subtracting satellite and receiver differential biases from the ionospheric observables.

Overall accuracy for absolute TEC values tends to be +/- 1-2 TECU. However, for our study we are interested in monitoring small-scale variations in ionospheric electron density, hence relative changes in TEC are our data set of interest, rather than absolute TEC values. The precision uncertainty for variations in TEC measurements using the GIM processing is typically of order +/- 0.01-0.1 TECU. [e.g., *Mannucci et al.,* 2004]

TEC Analysis

After processing the GPS RINEX files using the GIM software, we produce slant-TEC time series for the stations of interest in the time period when the first wave front of the tsunami is moving through the vicinity of the receivers.

We use two alternative methods to de-trend the TEC data, in order to focus on the perturbations to the background ionospheric electron density. First, we fit a polynomial to the TEC time series in order to fit the longer period variations, such as diurnal variations and elevation angle dependence of the TEC raypath. The polynomial fit is then subtracted from the actual data, leaving only the shorter-period perturbations. Second, we use a zero-phase bi-directional band-pass filter with a pass band of 0.5 to 5 mHz (corresponding to wave periods of 33.3 minutes to 3.3 minutes, a typical range of tsunami periods) to extract variations in TEC with periods similar to that of the ocean tsunami itself.

Fig. 1 shows an example of this analysis technique applied to the TEC time series from a single receiver-satellite pair. The upper plot shows absolute slant TEC (STEC) in the line-of-sight between the GEONET 0027 receiver and the SVN 54 GPS satellite, with a 10th order

polynomial fit to the measurements. The middle panel shows the residual differences between the polynomial fit and the actual observations. The bottom plot indicates the variations in band-pass-filtered TEC. Note the variations in TEC clearly visible in all three plots, ranging from ~ 15 minutes after the earthquake (~06:00 UT) to ~ 07 UT. This ionospheric perturbation, visible relatively soon after the earthquake, is likely caused by the acoustic wave generated by the earthquake itself. The F-region peak of the ionosphere was observed to be at ~300 km altitude based on electron density altitude profiles generated by the COSMIC satellite constellation. Similar variations during this time period are evident in TEC time series from many other GEONET GPS receivers at the same time. The perturbation to background TEC is quite distinct, but in order to determine whether it is caused by a tsunami, the earthquake itself, or some other phenomenon, we must analyze the data further to distinguish the horizontal speed of the traveling disturbance. This analysis requires an understanding of the phenomenology behind atmospheric wave propagation.

The F-region of the ionosphere, centered at 300-400 km altitude, depending on local time and latitude, contains the bulk of the free electrons in the ionosphere, and therefore makes the largest contribution to measurements of ionospheric TEC. Hence, any tsunami-driven atmospheric wave that could be visible as a variation in TEC would need to propagate from the ocean surface up to about 300-400 km altitude before TEC measurements could detect it.

Different types of atmospheric waves have different propagation velocities. A typical acoustic wave, often generated by the earthquake itself, propagates through the atmosphere at the sound speed, which varies from several hundred m/s near sea level to ~ 1 km/s at 400km altitude. It would take approximately 10 - 15 minutes for such a wave to affect the F-region, and thus TEC observations. The initial seismic source at the epicenter can generate an acoustic wave that propagates isotropically in the atmosphere, hence both vertical and horizontal propagation speeds would be the same (the sound speed of the atmosphere). By the time the wave reached the F-region, the horizontal velocity of the perturbation in TEC would be ~ 1 km/s. However, earthquakes also generate Rayleigh waves, transverse solid-Earth waves that propagate along the surface, with a horizontal velocity of about 3.4 km/s. These solid-Earth waves, also produce acoustic waves in the overlying atmosphere, and these acoustic waves propagate upward at the atmospheric

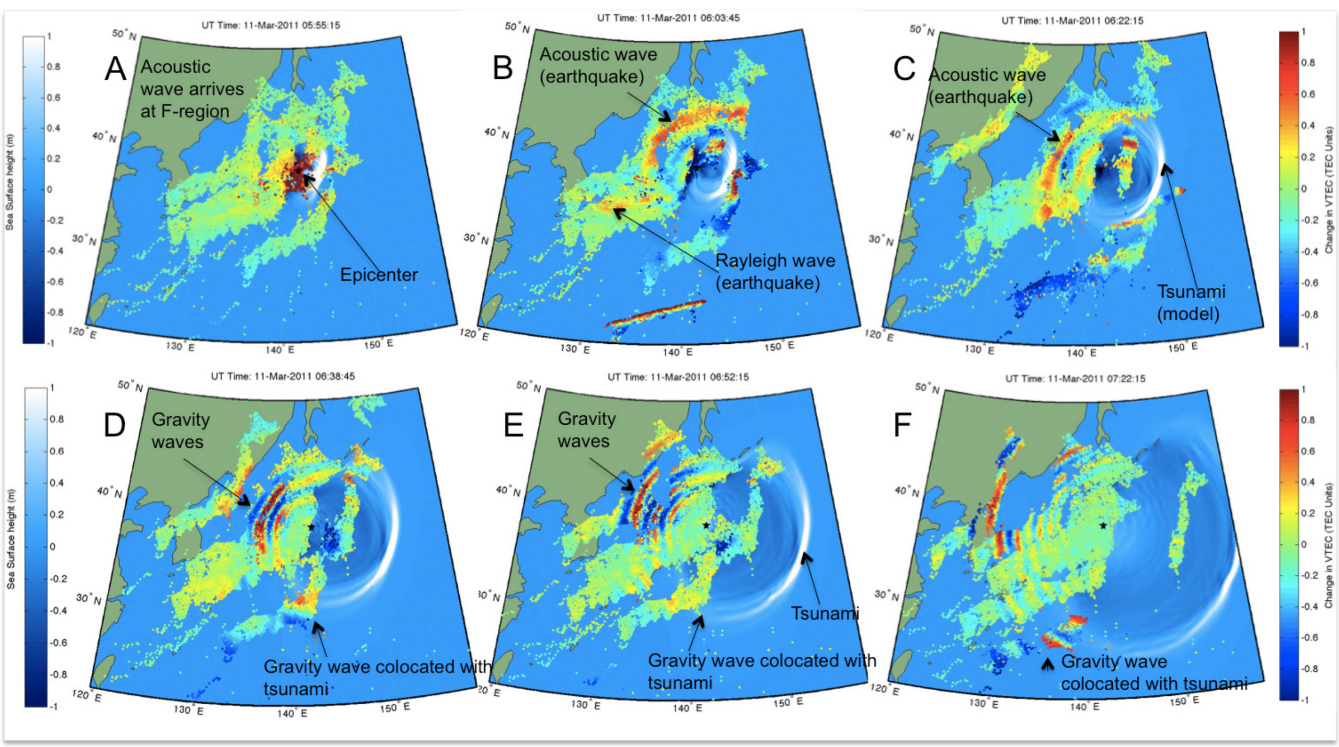

Fig 2. Map plots showing band-pass filtered VTEC at ionospheric pierce points (IPPs) above Japan at different times. Each cluster of IPPs represents locations in the ionosphere where the signal from one GPS satellite, communicating with all GEONET receivers, passes through the F-region peak at 300 km altitude. IPPs are plotted over sea surface heights from the Song tsunami model (in units of meters, left color bar) for comparison of wavefront positions in the ocean and ionosphere.

sound speed (~300 - 1000 m/s depending on altitude). As the wavefront of the Rayleigh wave moves horizontally along the land, new atmospheric acoustic waves are generated, such that the variation in electron density in the ionosphere would appear to be moving horizontally at 3.4 km/s, following the solid-Earth wave [*e.g., Hines,* 1972; *Artru et al.,* 2001; *Rolland et al.,* 2011]. Such earthquake-generated waves have been detected in ionospheric TEC in the past [*e.g., Calais and Minster,* 1995; *Kelley et al.,* 1985]. Earthquake-generated ionospheric disturbances must be considered because they could be mistaken for tsunami-driven signals, but would exist regardless of whether a tsunami was generated, since not all submarine earthquakes produce tsunamis.

Acoustic waves result in longitudinal compression in the direction of propagation. Internal gravity waves, on the other hand, are buoyancy waves resulting from vertical transverse oscillations of parcels of air caused by a slow rise and fall of the Earth's surface; in this case the ocean. Vertical propagation velocities for gravity waves vary with altitude, but it was previously thought that such waves would need at least 1.5 hours to propagate to the F-region peak [*Artru et al.,* 2005; *Galvan et al.,* 2011]. The horizontal velocity of observed perturbations will match the horizontal velocity of the disturbance itself. Ocean tsunamis tend to have speeds of ~200-300 m/s, depending on ocean depth [e.g., *Peltier and Hines*, 1976]. Thus, one way to distinguish signals associated with a tsunami from those associated with the earthquake itself is to look for coherent TEC variations, observed by multiple satellites and receivers, that are propagating at ~200-300 m/s in an outward direction from the tsunami's source. To distinguish the different types of acoustic and gravity waves moving through the ionosphere, we plot the band-pass filtered TEC perturbations in a way that allows us to easily identify signals with different speeds.

OBSERVATIONS NEAR THE EPICENTER

At 05:46:23 UT on March 11, 2011, a magnitude 9.0 earthquake struck at 38.3 north latitude, 142.4 deg east longitude, 129 km east of Sendai, in the region of Honshu, Japan. We used 1198 GEONET GPS stations to measure TEC perturbations within several thousand kilometers of the Tohoku epicenter. Figure 2 is a series of map plots showing the TEC disturbance in the region of Japan at different times. Each individual colored dot on the maps represents the ionospheric pierce point (IPP) at which the TEC raypath between one GPS satellite and one ground receiver penetrates the F-region peak at 300 km altitude. Hence, the dots show the location at which the integrated ionospheric electron density is most heavily influenced. Each Japan-shaped collection of dots represents one GPS satellite in communication with all 1198 GEONET receivers on the ground. The location of these IPPs moves from frame to frame as the GPS satellites position in the sky changes relative to the fixed GPS receivers. The color of the dots shows the band-pass filtered vertical TEC (VTEC, right-side color bar), similar to the bottom panel in Figure 1, except that the slant TEC has been mapped to vertical using a standard geometric mapping function in order to represent the TEC through the ionosphere along a theoretical vertical line-of-sight through a specific geographic position [*Komjathy et al.,* 2005].

In panel A, we see the first arrival of the acoustic waves at the ionosphere, roughly 10 minutes after the earthquake. In panel B, about 17 minutes after the seismic rupture, the fast Rayleigh wave is seen moving southwestward over Japan, and an acoustic wave is seen moving radially outward from the epicenter in all directions in Panels B and C. Panels D through F show TIDs traveling at the slower gravity wave speeds.
In addition to the ionospheric measurements, we also plot the Song model of tsunami sea surface height in blue (left-side color bar). We have done this to compare the position of the ocean tsunami itself to the ionospheric measurements of the TID. In several instances (Panels C, D, E, and F) there is a strong geographic correlation between the modeled tsunami and the ionospheric disturbances.

Map plots are useful for observing the overall behavior of the ionosphere in the region, but we are also interested in distinguishing those TIDs caused by the earthquake and those potentially caused by the tsunami, which may overlap one another in the maps. Figure 3 shows a series of plots which display the same band-pass filtered VTEC data as shown in Figure 2, but plotted as a function of great-circle distance from the epicenter and UT. The benefit of these "hodochron" plots is that a disturbance moving away from the epicenter (increasing along the vertical axis) over time (horizontal axis) will have a slope that can be interpreted as the velocity of that disturbance.

Figure 3A shows data from GPS SVN 55 only, with examples of three different wave speeds visible. The three black "guide" lines show sample velocities with different slopes: 3400 m/s for Rayleigh waves, 1000 m/s for acoustic waves, and 240 m/s for a typical gravity wave being driven by a tsunami. Colored disturbances in the band-pass filtered VTEC have slopes approximately parallel to these lines, and are labeled accordingly.
Figure 3B shows data from all available GPS satellites in the region. Since combining this data on a single plot necessitates data from some satellites covering data from others (IPPs at the same time and distance from the epicenter, but at different geographic locations will be plotted at the same coordinates in these plots), we plot these observations in order of absolute value, such that the highest magnitude perturbations are always visible on the top "layer". As in 3A, this plot shows Rayleigh and

acoustic waves that were likely generated by the earthquake, as well as gravity waves traveling at typical tsunami speeds. Interestingly, these gravity waves begin to appear in the ionosphere around 06:14 UT, approximately 30 minutes after the earthquake. This is somewhat surprising, as previous models have estimated that a gravity wave should take at least 1.5 hours to reach the F-region peak at 300 km altitude [*Galvan et al.,* 2011; *Hickey et al.,*2009; *Artru et al.,* 2005]. One possible explanation for this is that the atmospheric disturbance from the Tohoku event, being from a magnitude 9.0 earthquake and high amplitude tsunami, was significant enough to disturb the electron density of the ionospheric E-region, at roughly 100 km altitude, enough to be detectable in TEC. The maximum disturbances magnitudes range from 1-3 TECU (off scale high for this plot). With an average background VTEC value of ~30 TECU for Japan on this day, the perturbations represent up to 10% of the background ionospheric TEC.

Figure 3C shows the modeled sea surface height disturbance given by the Song tsunami model [e.g., *Song* 2007] for the Tohoku event. In this plot, unlike the others, the colors represent sea surface height in meters, rather than TEC perturbation. The first main wave front of the tsunami is visible as the strong linear pattern on the plot, approximately parallel to the 240 m/s guide line. The white squares represent DART buoys in the region near Japan, plotted at the time when each buoy first observed the tsunami and the distance from the epicenter.

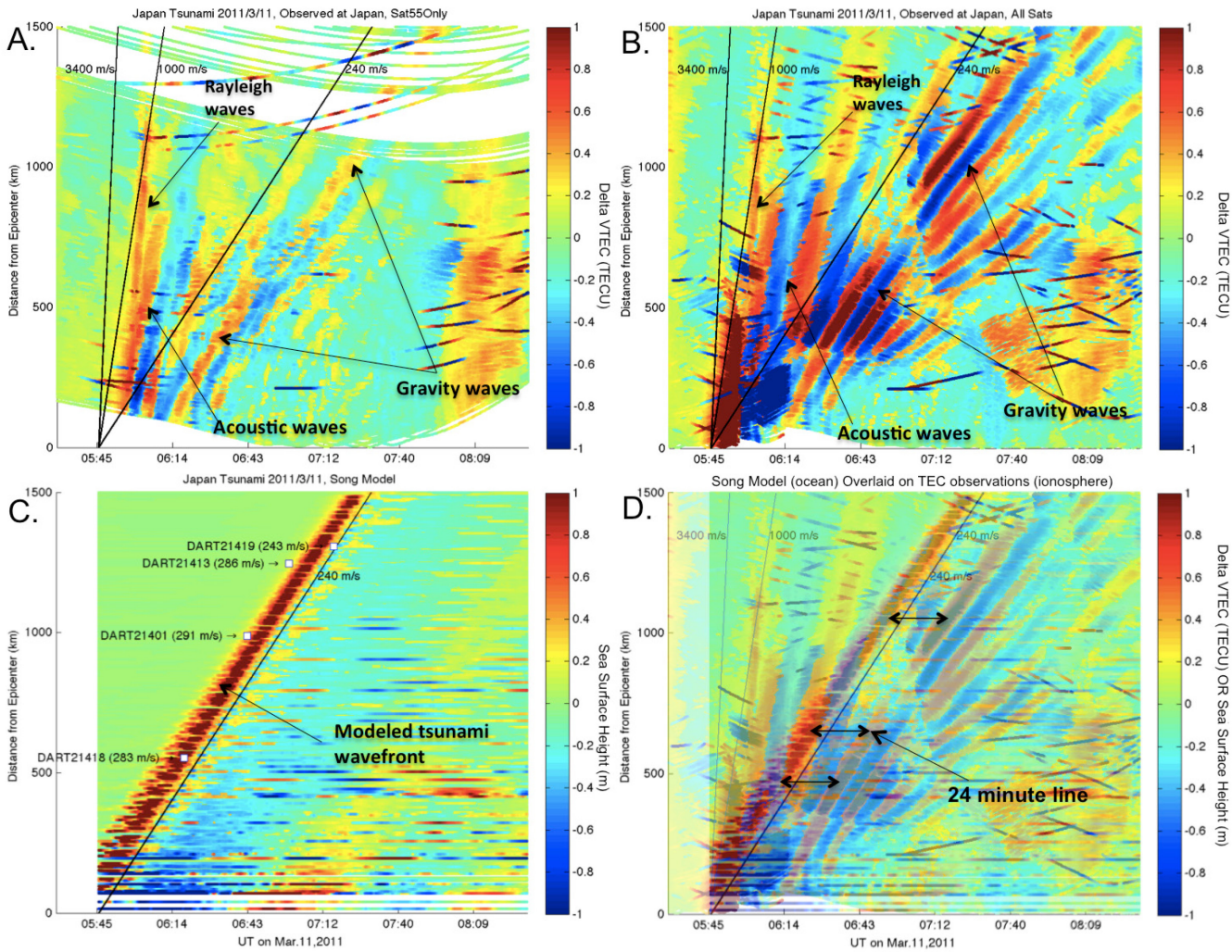

Fig 3. Hodochron plots for the near the Tohoku epicenter. Reference lines show the expected slope of waves traveling 3400 m/s (Rayleigh waves from the earthquake), 1000 m/s (acoustic waves from the earthquake), and 240 m/s (gravity waves from the tsunami). A.) Band-pass filtered VTEC perturbations for SVN 55 only, as a function of distance from the epicenter (vertical axis) and Universal Time (horizontal axis). B.) Band-pass filtered VTEC perturbations for all available GEONET stations (1198) and GPS satellites with elevation elevation angles > 30 deg. Highest amplitude variations are plotted on top layer to remain visible. C.) Song model [e.g., *Song* 2007] of sea surface height for the Tohoku tsunami. Color indicates sea surface height in meters. White squares show DART buoy position at time of tsunami arrival. D.) Panel C overlaid on panel B.

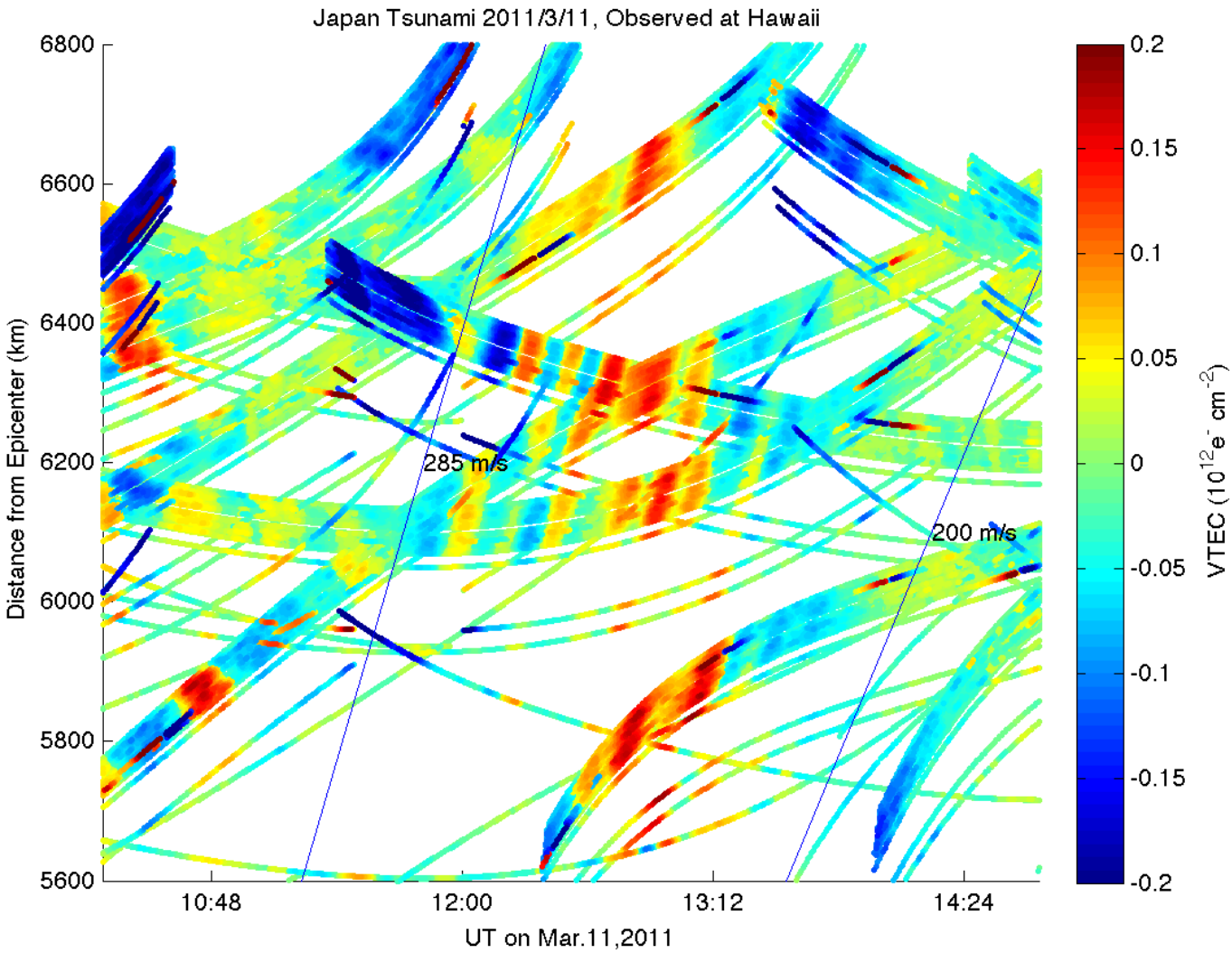

Fig. 4. Hodochron plot showing band-pass-filtered STEC for 67 GPS receivers on the Hawaiian Islands at the time the tsunami passage.

These in situ measurements of the tsunami demonstrate that the Song model provides a reasonable estimate of the actual tsunami characteristics. To compare the ocean tsunami with the behavior of the ionosphere, we overplot Figure 1C with 1B and show it as Figure 1D. The modeled ocean tsunami appears to have the same approximate slope, and hence velocity, as the first major wave front in the ionosphere, with a "lag" between the ocean tsunami and ionospheric wave of approximately 24 minutes. One interpretation of this is that, if looking at a particular geographic location, one would see the ocean wave pass by, and then the ionospheric disturbance pass by roughly 24 minutes later. This may be a result of the fact that the tsunami velocity varies with ocean depth, and the time for the gravity wave to reach the ionosphere such that it can affect TEC measurements is apparently at least ~30 minutes. Hence this offset between the locations of the wavefront in the ionosphere and at the ocean surface may be expected to vary at regions far afield from the epicenter.

We use the *Hickey et al*, [2009] atmosphere-ionosphere coupling model to produce an estimate of the expected perturbation to ionospheric TEC resulting from the known ocean tsunami amplitude, period, and azimuthal direction. This model numerically simulates the upward propagation of a spectrum of gravity waves in the atmosphere, and the interaction of those gravity waves with the ionosphere in the F-region. The model assumes a non-isothermal atmosphere, and takes into account such subtleties as eddy and molecular diffusion of heat and momentum, as well as ion drag, Coriolis force, and the altitude-variation of mean winds in the atmosphere.

To produce the initial perturbation of the lower boundary of the modeled atmosphere, we use sea surface height amplitudes associated with the tsunami at the location of

DART buoy #21413, which observed a tsunami speed of 284 m/s, a sea surface height amplitude of 0.76 m, and a period of 32 minutes off the southeast coast of Japan [http://www.ndbc.noaa.gov/dart.shtml]. Using this as input to the *Hickey et al.,* [2009] model, we find an expected vertical TEC perturbation of 5.3% of the background TEC. Analysis of our observed TEC perturbations in the region near DART 21413 reveals TEC perturbations between 0.2 and 3 TECU, at a region and time where the background TEC was approximately 32 TECU. This yields a range of observed TEC perturbations of 0.63% to 9.4 %. The model-estimated TEC perturbation (5.3%) falls within that range. Additional modeling efforts of this type are warranted to gain further insight. A similar analysis was performed for the Chile 2010 tsunami as observed at the same buoy, DART 21413, and is discussed in *Galvan et al.,* [2011].

OBSERVATIONS FAR AFIELD

We used 67 receivers on the Hawaiian Islands to observe the TIDs as the tsunami arrived in that region. Figure 4 shows a hodochron plot similar to Figure 1B, but in the region of Hawaii. The gaps in data coverage (white space on the plot) are due to the fewer GPS receivers in Hawaii as compared to Japan. Two guide line with slopes of 285 m/s and 200 m/s show a range of expected tsunami amplitudes at this location. Acoustic and Rayleigh waves would have long since passed the Hawaiian Islands by this time, and so no guide-lines for those higher speed waves are visible on the plot. Note that are several coherent perturbations to band-pass filtered VTEC visible between 12 and 13 UT, which have slopes (velocities) in the appropriate range for gravity waves driven by a tsunami. While these perturbations are significantly smaller in magnitude than those observed near the epicenter (~0.2 TECU), note that this region was in a pre-dawn local time when the tsunami passed by (Hawaii-Aleutian Standard Time = UT – 10 hours). Hence this observation demonstrates that, at least for tsunamis of this magnitude, the gravity wave is detectable even in the tenuous nighttime ionosphere.

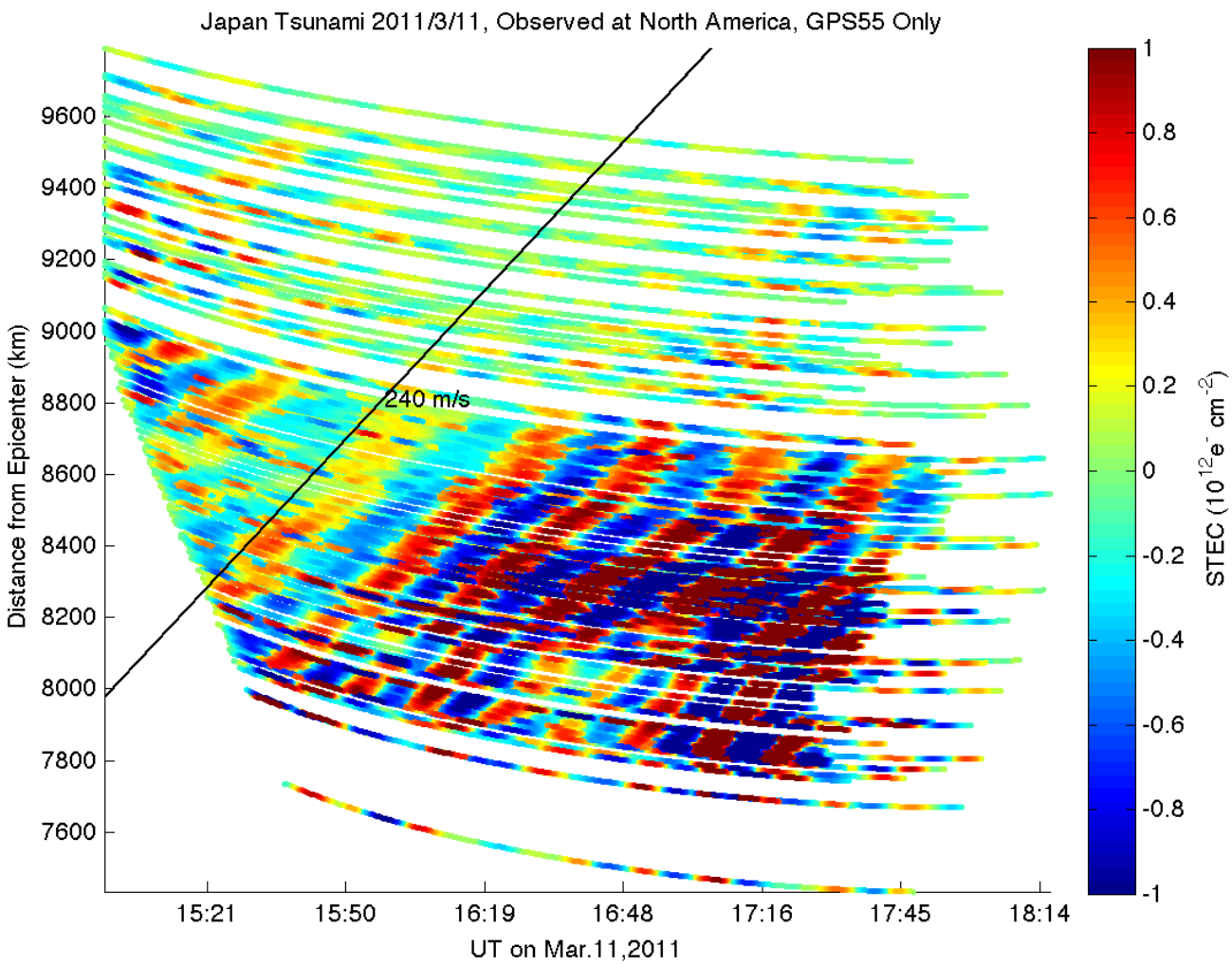

Fig. 5: Hodochron plot showing band-pass filtered TEC for a single satellite (GPS SVN 55) and 178 receivers in the Plate Boundary Observatory network in western North America. Line shows horizontal velocity of gravity waves (240 m/s).

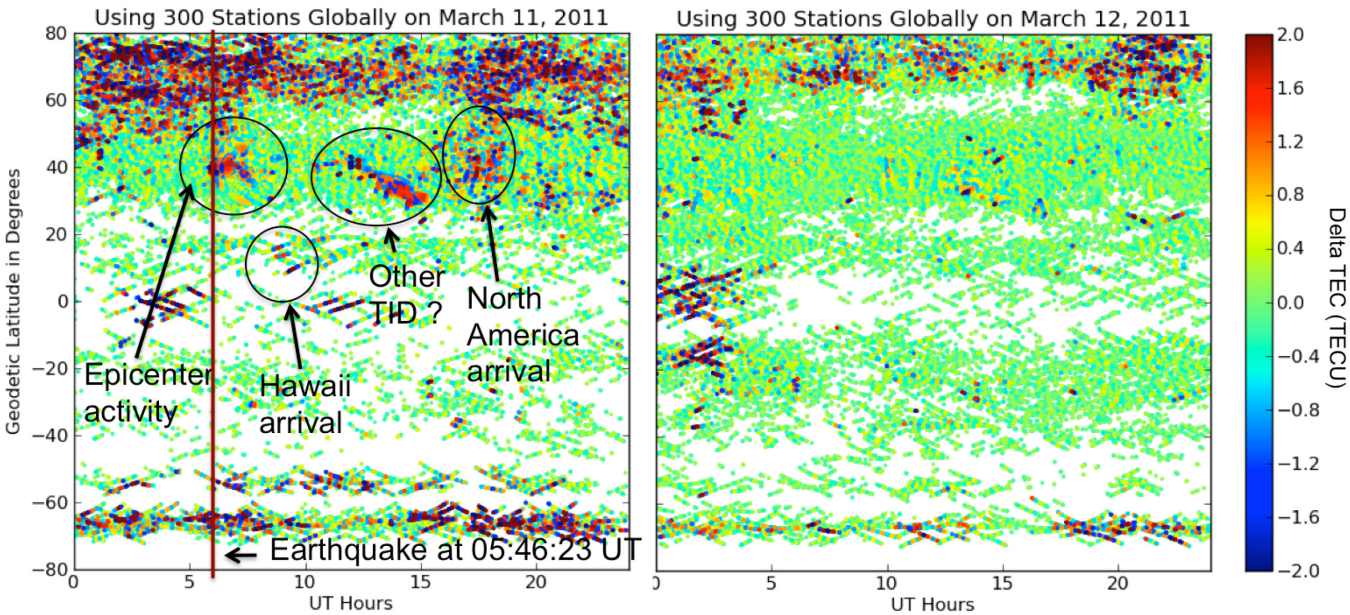

Fig. 6: Band-pass filtered TEC from 300 GPS receivers spread throughout the globe, plotted in color as a function of latitude and time. Traveling ionospheric disturbances (TIDs) are visible at various times and locations.

In North America, the Plate Boundary Observatory consists of over 700 GPS stations spread throughout the western region of the continent. Here we show a sample of the TEC data from this network. Figure 5 shows the band-pass filtered TEC on another hodochron plot, for only one GPS satellite (SVN 55) and a subset of 178 GPS receivers distributed throughout the region. Again, a clear signature of a TID traveling away from the Tohoku epicenter at approximately the same speed as the tsunami is visible in the ionospheric data. Interestingly, while the ocean tsunami stops at the American west coast, the atmospheric gravity wave likely continues to propagate over the continent for some distance. The extent of this continued propagation over land after the driving tsunami has been halted is the subject of ongoing investigation.

GLOBAL OBSERVATIONS

These observations suggest that the ionospheric signature of ocean tsunamis can indeed be remotely observed, however there are other sources for TIDs not associated with tsunamis, such as intense tropospheric weather [*Hung et al.,* 1978, *Kelley* 1997; *Xiao et al.,* 2007], geomagnetic and auroral activity [*Richmond and Matsushita*, 1975; *Nicolls et al.,* 2004], and earthquakes [*Calais and Minster*, 1995; *Artru et al.,* 2001; *Kelley et al.,* 1985]. The existence of non-tsunami-driven TIDs can make detection and confirmation of tsunami association more challenging. In our current research, we distinguish ionospheric signatures of tsunami-driven TIDs by verifying that the horizontal speed and direction of the TIDs match that of the ocean tsunami. However, to provide more perspective on just how frequent such non-tsunami-driven TIDs are in the ionosphere, we apply the same data analysis strategy to 300 GPS stations spread throughout the globe. Figure 6 shows band-pass filtered TEC for these stations in color as a function of latitude (y-axis) and UT (x-axis) for March 11 (left panel) and March 12 (right panel). There was a significant geomagnetic storm on March 11, which explains the abundant TEC perturbations in the auroral regions visible at high latitudes in the left panel. March 12 was a geomagnetically quiet day by comparison. On March 11, strong TEC perturbations are seen between latitudes 30 and 45 north (the region of Japan) immediately following the earthquake, corresponding to the earthquake and tsunami-driven TIDs discussed earlier in this paper. There are also TEC perturbations visible at latitudes ~20 deg and below near the time of the tsunami's passage by the Hawaiian islands. Only a few GPS receivers in Hawaii were used for this global survey, which may explain why a stronger signal is not observed around UT 12-13, corresponding to our Hawaii observations presented earlier. We also note strong perturbations around 40 deg North latitude between UT 15 and 20, which may correspond to the arrival of the tsunami-driven TID at North America.

It is also important to note that there are TIDs evident in this global survey that seem to be unrelated to the earthquake or tsunami. One example is a TID visible around 40 deg north latitude between 12 and 15 UT. Though not shown here, we have investigated this TID, which is detected by the GEONET network at Japan, and found it to be an ionospheric disturbance that originates north of Japan and moves southwest past the epicenter.

This wave seems to have no relation to the earthquake or tsunami, and yet it is still oscillating in the 0.5 - 5 mHz pass-band we use to filter the data. Such observations highlight the need for additional information if this method is to be used for real-time monitoring of tsunami-driven gravity waves in the future. Acquiring such additional information is likely to be feasible. For example, the USGS routinely posts an approximate epicenter location and earthquake magnitude within a few minutes of rupture. A future ionosphere-monitoring system could begin monitoring TEC data from the region near the epicenter soon after the seismic disturbance occurs, and the expected direction of "candidate" tsunami or earthquake driven signals could be constrained based on the epicenter location.

DISCUSSION AND CONCLUSIONS

There are potential applications in real-time tsunami monitoring and early warning using this analysis method. Our current technique is a method for analyzing historical ionospheric disturbances after a tsunami has occurred. In the future, we hope to develop algorithms that will begin monitoring TEC in real time in the region of a seismic source that could produce a tsunami. Due to the geometry involved in TEC raypaths between GPS satellites and ground-based receivers, a disturbance in electron density moving through the ionosphere can be observed from many hundreds of km away (horizontally), allowing the GPS receiver to detect the tsunami-driven variation before the ocean tsunami itself arrives at the shore. Though the ability to make such observations using TEC will vary on a case by case basis, this demonstrates that future systems that monitor real-time TEC immediately after a major earthquake could contribute additional early information to an existing tsunami warning system such as that employed by the Pacific Tsunami Warning Center, which currently uses modeled tsunami propagation models and DART buoy and tidal gauge observations. As additional GPS receivers are displayed, and additional GNSS services become available (GLONASS, Galileo, COMPASS, etc.), there is a high likelihood that more data will be made available for this type of remote sensing in the future.

In addition, space-based GPS receivers used in radio occultation studies, such as those on the COSMIC satellite constellation, have been shown to contribute useful ionospheric TEC information to improve model-estimated altitude electron density profiles [e.g., *Komjathy et al.,* 2010]. Future study is required to determine whether COSMIC observations may be useful for variations in electron density over a limited geographic region, given the geometry of estimating TEC along the radio signal ray path from the LEO satellite, through the ionosphere, and back out to space to a GPS satellite.

In summary, we have shown observational evidence of variations in GPS TEC measurements that are concurrent with the Tohoku tsunami of March 11, 2011. TIDs consistent with internal gravity waves caused by the Tohoku tsunami are visible in at least three regions: Japan, Hawaii, and the western region of North America. The observations near the epicenter represent the strongest tsunami-driven ionospheric disturbance seen to date. Future efforts will apply these research techniques to additional tsunami events to further improve our ability to detect and identify tsunami-driven ionospheric disturbances in GPS TEC data. While the scientific questions regarding the nature of this coupling between the ocean and ionosphere are still being studied, our research efforts should contribute toward the development of a future TEC monitoring system that takes advantage of existing real-time networks of GPS receivers, such as the NASA Global Differential GPS System (http://www.gdgps.net). Such a system could provide additional information on the inferred amplitude, period, and velocity of a tsunami, based on the observed parameters of the ionospheric internal gravity wave.

ACKNOWLEDGMENTS

The authors would like to thank Dr. John LaBrecque of NASA Headquarters and the Earth Science and Interior NASA ROSES Grant (NNH07ZDA001N-ESI), which made this research possible. Tony Mannucci and Mark Butala also provided useful suggestions which improved this paper. RINEX files from the Japanese GEONET network were provided by the Geospatial Information Authority (GSI), a part of the Japanese Ministry of Land, Infrastructure, Transport and Tourism (http://terras.gsi.go.jp/gps/geonet_top.html). This research was performed at the Jet Propulsion Laboratory, California Institute of Technology under contract to the National Aeronautics and Space Administration.

REFERENCES

Artru, J., P. Lognonné, and E. Blanc (2001), Normal modes modeling of post-seismic ionospheric oscillations, *Geophysical Research Letters*, *28*, 697–700, 10.1029/2000GL000085.

Artru, J., V. Ducic, H. Kanamori, P. Lognonné, and M. Murakami (2005), Ionospheric detection of gravity waves induced by tsunamis, *Geophysical Journal International*, *160*, 840–848, 10.1111/j.1365-246X.2005.02552.x.

Calais, E., and J.B. Minster (1995), GPS detection of ionospheric perturbations following the January 17, 1994, Northridge earthquake, *Geophys. Res. Lett.*, 22, 1045-1048, 10.1029/95GL00168.

Galvan, D. A., A. Komjathy, M. P. Hickey, and A. J. Mannucci (2011), The 2009 Samoa and 2010 Chile tsunamis as observed in the ionosphere using GPS total electron content, *Journal of Geophysical Research (Space Physics)*, *116*, A06,318, 10.1029/2010JA016204.

Hickey, M. P., G. Schubert, and R. L. Walterscheid (2009), Propagation of tsunami-driven gravity waves into the thermosphere and ionosphere, *J. Geophys. Res.*, 114, A08304, doi:10.1029/2009JA014105.

Hines, C. O. (1972), Gravity Waves in the Atmosphere, *Nature*, *239*, 73–78, 10.1038/239073a0.

Hung, R. J., T. Phan, and R. E. Smith (1978), Observation of gravity waves during the extreme tornado outbreak of 3 April 1974, *Journal of Atmospheric and Terrestrial Physics*, *40*, 831–843.

Kelley, M. C. (1997), In situ ionospheric observations of severe weather-related gravity waves and associated small-scale plasma structure, *Journal of Geophysical Research*, *102*, 329–336, 10.1029/96JA03033.

Kelley, M. C., R. Livingston, and M. McCready (1985), Large amplitude thermospheric oscillations induced by an earthquake, *Geophysical Research Letters*, *12*, 577–580, 10.1029/GL012i009p00577.

Komjathy, A., B. Wilson, X. Pi, V. Akopian, M. Dumett, B. Iijima, O. Verkhoglyadova, and A. J. Mannucci (2010), JPL/USC GAIM: On the impact of using COSMIC and ground-based GPS measurements to estimate ionospheric parameters, *Journal of Geophysical Research (Space Physics)*, *115*, 2307, 10.1029/2009JA014420.

Komjathy, A., L. Sparks, B. D. Wilson, and A. J. Mannucci (2005), Automated daily processing of more than 1000 ground-based GPS receivers for studying intense ionospheric storms, *Radio Sci.*, 40, RS6006, doi:10.1029/2005RS003279.

Liu, J.-Y., C.-H. Chen, C.-H. Lin, H.-F. Tsai, C.-H. Chen, and M. Kamogawa (2011), Ionospheric disturbances triggered by the 11 march 2011 M9.0 Tohoku earthquake, *J. Geophys. Res.*, *116*(A6), 10.1029/2011JA016761.

Mai, C. L., and J. F. Kiang (2009), Modeling of ionospheric perturbation by 2004 Sumatra tsunami, *Radio Science*, *44*, 3011, 10.1029/2008RS004060.

Mannucci, A. J., B. D. Wilson, D. N. Yuan, C. H. Ho, U. J. Lindqwister, and T. F. Runge (1998), A global mapping technique for GPS-derived ionospheric total electron content measurements, *Radio Science*, *33*, 565–582, 10.1029/97RS02707.

Mannucci, A. J., G. A. Hajj, B. A. Iijima, A. Komjathy, T. K. Meehan, X. Q. Pi, J. Srinivasan, B. T. Tsurutani, B. Wilson, L. D. Zhang, and M. Moldwin (2004), GPS-based remote sensing of the geospace environment: horizontal and vertical structure of the ionosphere and plasmasphere, in *Society of Photo-Optical Instrumentation Engineers (SPIE) Conference Series*, *Society of Photo-Optical Instrumentation Engineers (SPIE) Conference Series*, vol. 5660, edited by C. A. Nardell, P. G. Lucey, J. H. Yee, and J. B. Garvin, pp. 1–13, 10.1117/12.580048.

Nicolls, M. J., M. C. Kelley, A. J. Coster, S. A. González, and J. J. Makela (2004), Imaging the structure of a large-scale TID using ISR and TEC data, *Geophysical Research Letters*, *31*, 9812, 10.1029/2004GL019797.

Occhipinti, G., P. Lognonné, E. A. Kherani, and H. Hébert (2006), Three-dimensional waveform modeling of ionospheric signature induced by the 2004 Sumatra tsunami, *Geophysical Research Letters*, *33*, L20,104, 10.1029/2006GL026865.

Occhipinti, G., E. A. Kherani, and P. Lognonné (2008), Geomagnetic dependence of ionospheric disturbances induced by tsunamigenic internal gravity waves, *Geophysical Journal International*, *173*, 753–765, 10.1111/j.1365-246X.2008.03760.x

Peltier, W. R., and C. O. Hines (1976), On the possible detection of tsunamis by a monitoring of the ionosphere, *Journal of Geophysical Research*, *81*, 1995–2000, 10.1029/JC081i012p01995.

Richmond, A. D., and S. Matsushita (1975), Thermospheric response to a magnetic substorm, *Journal of Geophysical Research*, *80*, 2839–2850, 10.1029/JA080i019p02839.

Rolland, L. M., P. Lognonné, and H. Munekane (2011), Detection and modeling of Rayleigh wave induced patterns in the ionosphere, *Journal of Geophysical Research (Space Physics)*, *116*, A05,320, 10.1029/2010JA016060.

Rolland, L. M., G. Occhipinti, P. Lognonné, and A. Loevenbruck (2010), Ionospheric gravity waves detected offshore Hawaii after tsunamis, *Geophys. Res. Lett.*, *37*, 17,101, 10.1029/2010GL044479.

Song, Y. T. (2007), Detecting tsunami genesis and scales directly from coastal GPS stations, *Geophys. Res. Lett.*, *34*, L19,602, 10.1029/2007GL031681.

Xiao, Z., S. Xiao, Y. Hao, and D. Zhang (2007), Morphological features of ionospheric response to typhoon, *Journal of Geophysical Research (Space Physics)*, *112*, 4304, 10.1029/2006JA011671.